

# Spectra of $W^{39+}$ - $W^{47+}$ in the 12 nm to 20 nm region observed with an EBIT light source

Yu Ralchenko, J Reader, JM Pomeroy, JN Tan, and JD Gillaspy

National Institute of Standards and Technology, Gaithersburg MD 20899-8422, USA

E-mail: [yuri.ralchenko@nist.gov](mailto:yuri.ralchenko@nist.gov)

**Abstract.** We observed spectra of highly ionized tungsten in the extreme ultraviolet with an electron beam ion trap (EBIT) and a grazing incidence spectrometer at the National Institute of Standards and Technology. Stages of ionization were distinguished by varying the energy of the electron beam between 2.1 keV and 4.3 keV and correlating the energies with spectral line emergence. The spectra were calibrated by reference lines of highly ionized iron produced in the EBIT. Identification of the observed lines was aided by collisional-radiative modeling of the EBIT plasma. Good quantitative agreement was obtained between the modeling results and the experimental observations. Our line identifications complement recent results for  $W^{40+}$ - $W^{45+}$  observed in a tokamak plasma by Pütterich *et al* (*J. Phys. B: At. Mol. Opt. Phys.* **38**, 3071, 2005). For most lines we agree with their assignment of ionization stage. Additionally, we present new identifications for some allowed and forbidden lines of  $W^{39+}$ ,  $W^{44+}$ ,  $W^{46+}$ , and  $W^{47+}$ . The uncertainties of our wavelengths range from 0.002 nm to 0.010 nm.

PACS numbers: 32.30.Jc,39.10.+j

Submitted to: *J. Phys. B: At. Mol. Phys.*

## 1. Introduction

Spectra of highly ionized tungsten continue to be of interest for the development of magnetic fusion energy. Tungsten is considered a strong candidate for use as a plasma-facing material in advanced tokamaks such as ITER. Furthermore, accurately measured spectra of highly-charged ions serve as a test-bed for advanced atomic structure and plasma kinetics codes.

Spectra of highly-ionized tungsten in the 4 nm to 14 nm region, observed in the ASDEX Upgrade tokamak in Garching, Germany, were recently reported by Pütterich *et al* [1]. This tokamak had part of its first wall coated with tungsten. In the 12 nm -14 nm region twelve lines of  $W^{40+}$ - $W^{45+}$  were identified. In that measurement, the lines were observed with a 2.2 m grazing incidence spectrometer. Ionization stages were identified by observing the evolution of the lines during the tokamak discharge. The wavelength uncertainty was given as  $\pm 0.005$  nm. These observations made it possible for the authors of Ref. [1] to resolve a number of questions that had been raised about line identifications in W spectra from earlier tokamak work [2].

In the present work we observed highly ionized W using the electron beam ion trap (EBIT) operating at the National Institute of Standards and Technology (NIST). This work is an extension to longer wavelengths of our recent study [3] of the x-ray spectra of W. The present spectra were observed in the (4-20) nm region with the grazing incidence spectrometer [4]. As the (4-8.5) nm spectrum of tungsten was well covered in a recent report from EBIT-II at Lawrence Livermore National Laboratory [5], we concentrate primarily on the spectra in the longer wavelength region. These measurements complement the tokamak work [1] and the new compilation of spectra for all W ions from  $W^{2+}$  to  $W^{73+}$  [6].

## 2. Experiment

Highly ionized iron and tungsten were produced in the NIST EBIT. The EBIT is a versatile light source, capable of producing nearly any ion charge state of nearly any element. The EBIT's electron beam has a very narrow energy distribution ( $\lesssim 60$  eV) [7] that allows precise control of the charge state distribution in the trap. A detailed description of the NIST EBIT and its performance is given by one of us elsewhere [9]. Other pertinent EBIT parameters in this experiment are a 220 V trap depth, 2.7 T magnetic flux density, 4 s trap reloading period, and  $< 2 \times 10^{-3}$  Pa injected gas reservoir pressure (P1, outer chamber of gas injector, see Ref. [8] for gas injector description; in the present work, the diameter of the injector aperture was 3/16 inch, and the inner diameter of the nozzles were 1/8 inch) on a nominal background pressure inside the ion trap of  $< 5 \times 10^{-9}$  Pa. For the present experiment, the tungsten atoms were injected into the plasma by a metal vapor vacuum arc (MEVVA) ion source [10]. The MEVVA uses eight cathodes, any one of which can be quickly selected without disturbing any other experimental conditions. This helps to minimize systematic errors in the calibration.

The spectra were recorded using a flat-field spectrometer recently deployed on this facility. It is described thoroughly in a separate report [4]. Briefly, it consists of a spherical focusing mirror, a bilateral entrance slit, a gold-coated concave grating, and a liquid-nitrogen-cooled detector. The focusing mirror has a radius of curvature of 9171 mm and is used at a grazing angle of  $3^\circ$ . Together these components maximize the light collection efficiency while maintaining moderately good spectral resolution. The diffraction grating, which is the type designed by Harada and Kita [11], has a radius of curvature of 5649 mm and a variable groove spacing averaging 1200 lines/mm. When used at a grazing angle of  $3^\circ$ , the reciprocal linear dispersion at 12 nm is about 0.6 nm/mm. The detector is a back-illuminated charge-coupled device (CCD) camera placed at the grating's focal surface. The CCD consists of a  $1340 \times 400$  array of pixels that are directly exposed to extreme ultraviolet (EUV) radiation. The signals are column-summed in hardware to minimize read-out noise. Observations of the full frame exhibit negligible spectral line curvature. The instrument's resolution as configured for this experiment is about 350, corresponding to a resolving limit of about 0.03 nm.

Light from wavelengths above 25 nm was filtered out by a zirconium foil placed between the EBIT and the grazing-incidence focusing mirror. An efficiency curve for the entire spectral recording system (including filter) is shown by the dashed line in Fig. 1. As seen, the system has good transmission between 6 and 18 nm. The maximum transmission is about 60 % at 10 nm [4]. Even without the Zr filter, as shown in Ref. [4], the detection efficiency of the spectrometer falls off rapidly below 8 nm.

The tungsten spectra were calibrated by lines of  $Fe^{17+}$ - $Fe^{22+}$ , with wavelengths taken from the NIST Atomic Spectra Database (ASD) [12]. For the calibration spectra, iron was injected into the EBIT plasma periodically during the course of experimental runs. The iron ions were excited at several beam energies between 1.8 keV and 2.9 keV. We also used spectral lines of  $O^{4+}$  and  $O^{5+}$ , with wavelengths taken from ASD, as well as second order lines of W in the 6 nm to 8 nm region, with wavelengths taken from Ref. [5]. The oxygen was likely introduced into the plasma through a side port, to which another spectrometer was connected.

In order to distinguish stages of ionization, we took a series of spectra at nineteen different beam energies between 2.0 keV and 4.3 keV. The emergence of new spectral lines as the energy was changed was correlated with the ionization energies of the tungsten ions. The ionization energies of the ions relevant to this work as determined by Kramida and Reader [13] are shown in Table 1. Our ionization stage assignments were also correlated with the stages of lines in the 4 nm to 8 nm region given in Ref. [5], where a similar method was used.

The spectra were measured during two separate runs. The first one (run A) covered 13 beam energies from 2001 eV to 3113 eV. Spectra from this run are shown in Figs. 1 and 2 after a background (dominated by essentially noiseless CCD bias) of approximately 4000 counts/channel was subtracted. The second run (run B) covered 6 energies from 2885 eV to 4228 eV, as shown in Fig. 3. The nominal beam energies and currents are presented in Table 2. In what follows, the spectra will be referred to by the beam energy

**Table 1.** Ionization potentials (in eV) of W ions.

Ion	Sequence	Ground state configuration	Ref. [13]	Present work (calculated)
$W^{40+}$	Se	$4s^24p^4$	$1940.6 \pm 2.0$	1944
$W^{41+}$	As	$4s^24p^3$	$1994.8 \pm 2.0$	1997
$W^{42+}$	Ge	$4s^24p^2$	$2149.2 \pm 2.1$	2147
$W^{43+}$	Ga	$4s^24p$	$2210.0 \pm 1.5$	2206
$W^{44+}$	Zn	$3d^{10}4s^2$	$2354.5 \pm 1.4$	2354
$W^{45+}$	Cu	$3d^{10}4s$	$2414.1 \pm 0.4$	2415
$W^{46+}$	Ni	$3d^{10}$	$4057 \pm 3$	4052
$W^{47+}$	Co	$3d^9$	$4180 \pm 4$	4173
$W^{48+}$	Fe	$3d^8$	$4309 \pm 4$	4304

**Table 2.** Nominal beam energies (in eV) and currents (in mA) for runs A and B.

Run A				Run B	
Energy	Current	Energy	Current	Energy	Current
2001	28.9	2600	32.9	2885	52.0
2083	31.5	2687	32.9	3310	67.0
2169	32.5	2773	32.6	3513	78.0
2255	32.5	2858	32.6	3740	85.5
2341	32.7	2941	32.7	4080	94.5
2429	32.8	3113	32.7	4228	103.0
2515	32.9				

followed by the run identification, e.g., 2001A. For completeness and easier identification of the higher-order lines, the figures show the whole spectral range from 4 nm to 20 nm.

### 3. Calculations of spectra

Similar to our work on x-ray emission [3], the analysis of the EUV spectra was aided by collisional-radiative (CR) modeling of the EBIT plasma. The non-Maxwellian CR code NOMAD [14] was used to calculate the level populations and line intensities for various electron beam energies. The electron density was fixed in the model at  $N_e = 10^{11} \text{ cm}^{-3}$ . Test runs showed that the modeling results are not sensitive to the value of  $N_e$  in the range  $10^{11} \text{ cm}^{-3}$  to  $10^{12} \text{ cm}^{-3}$ .

Since the atomic data required for the CR modeling of highly-charged tungsten are not available in the literature, we performed large-scale calculations of all relevant parameters, i.e., energy levels, radiative transition probabilities (including forbidden transitions), and collisional cross sections, using the relativistic Flexible Atomic Code (FAC). The FAC methods and techniques, which are described in detail in Ref. [15], are highly suitable for multiply-charged ions of heavy elements, clearly of great importance

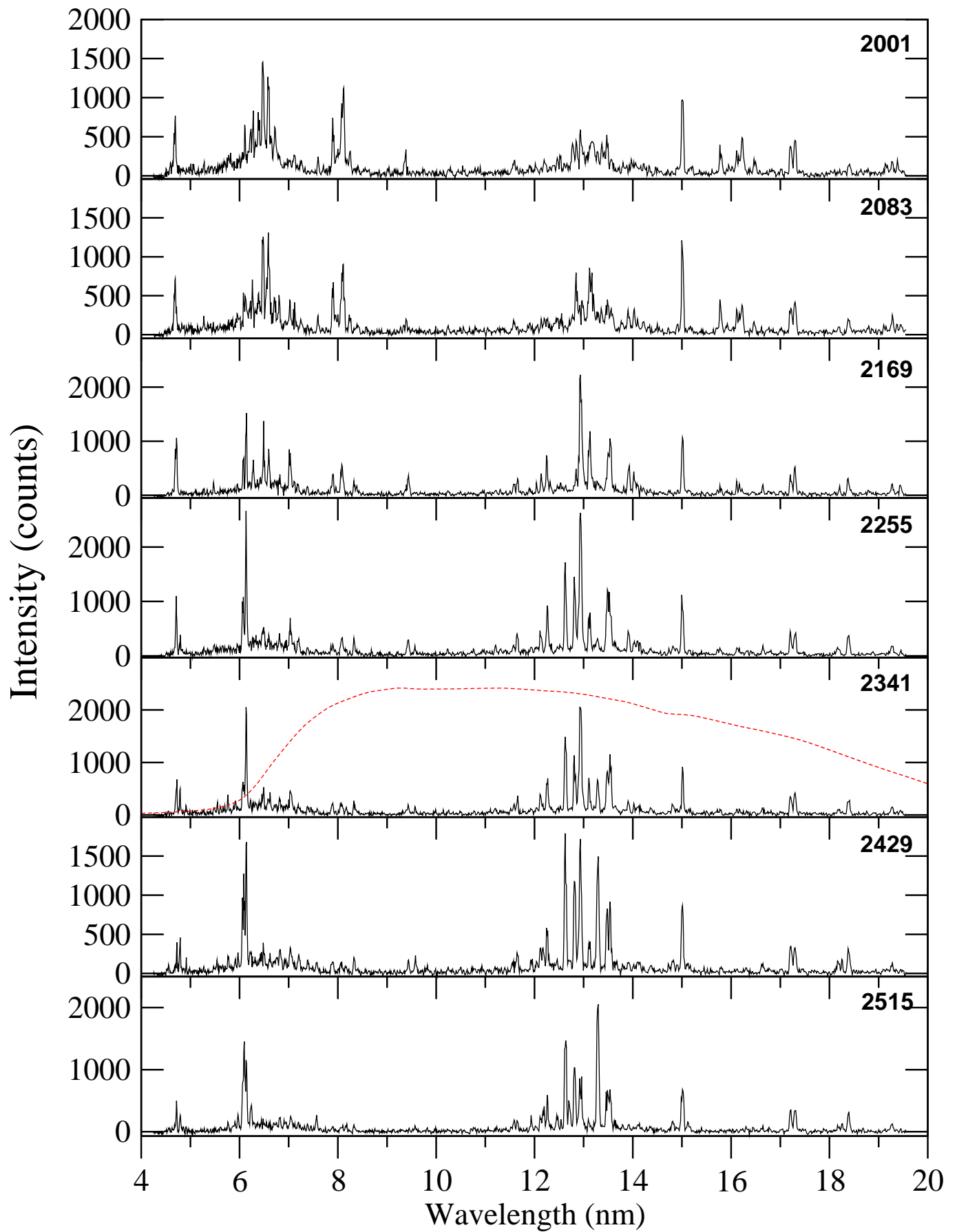


**Figure 1.** Experimental spectra for low beam energies of run A. The dashed line represents a relative efficiency curve for the spectrometer.

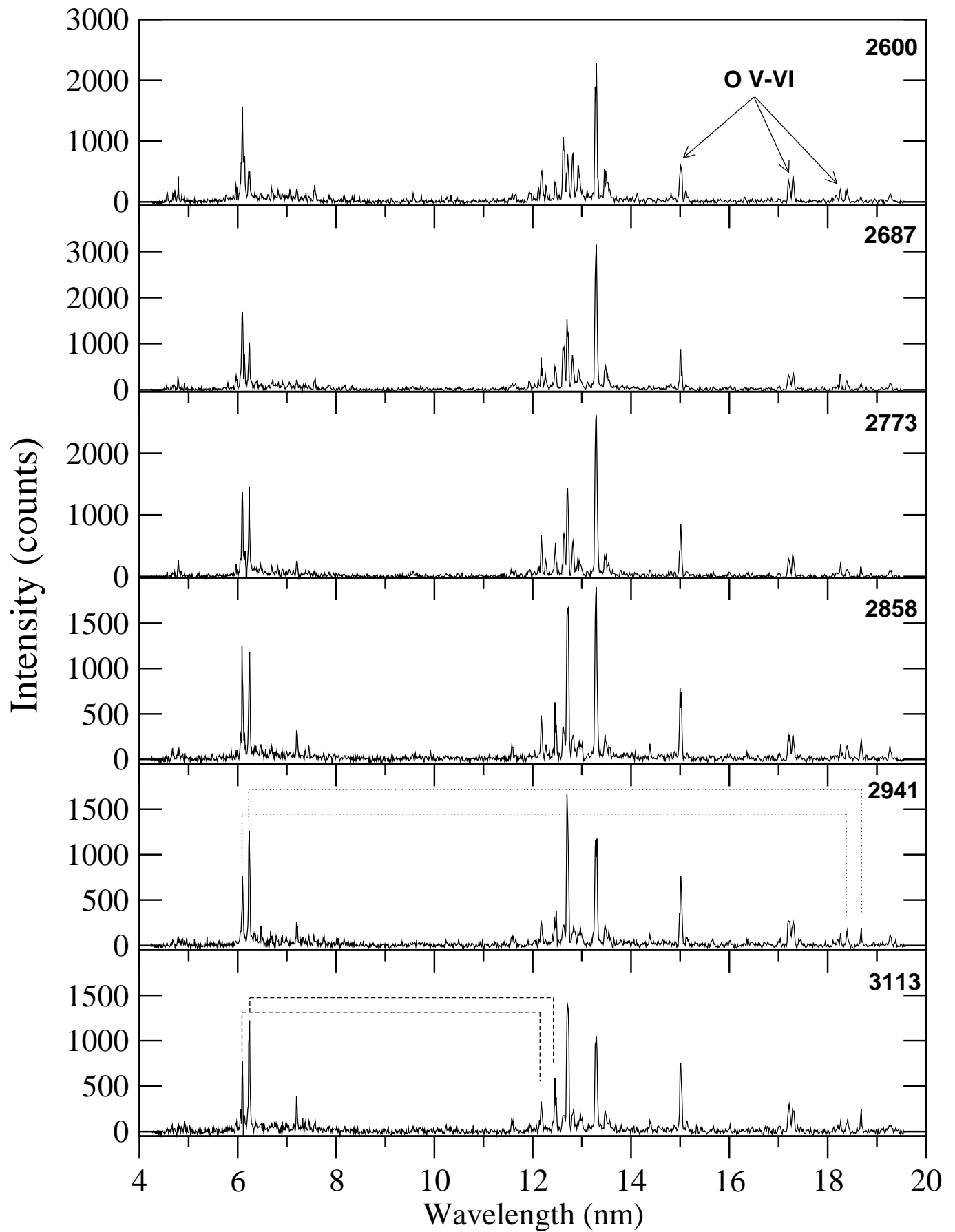


**Figure 2.** Experimental spectra for high beam energies of run A. Examples of higher order spectral lines are indicated by dashed (second-order) and dotted (third-order)

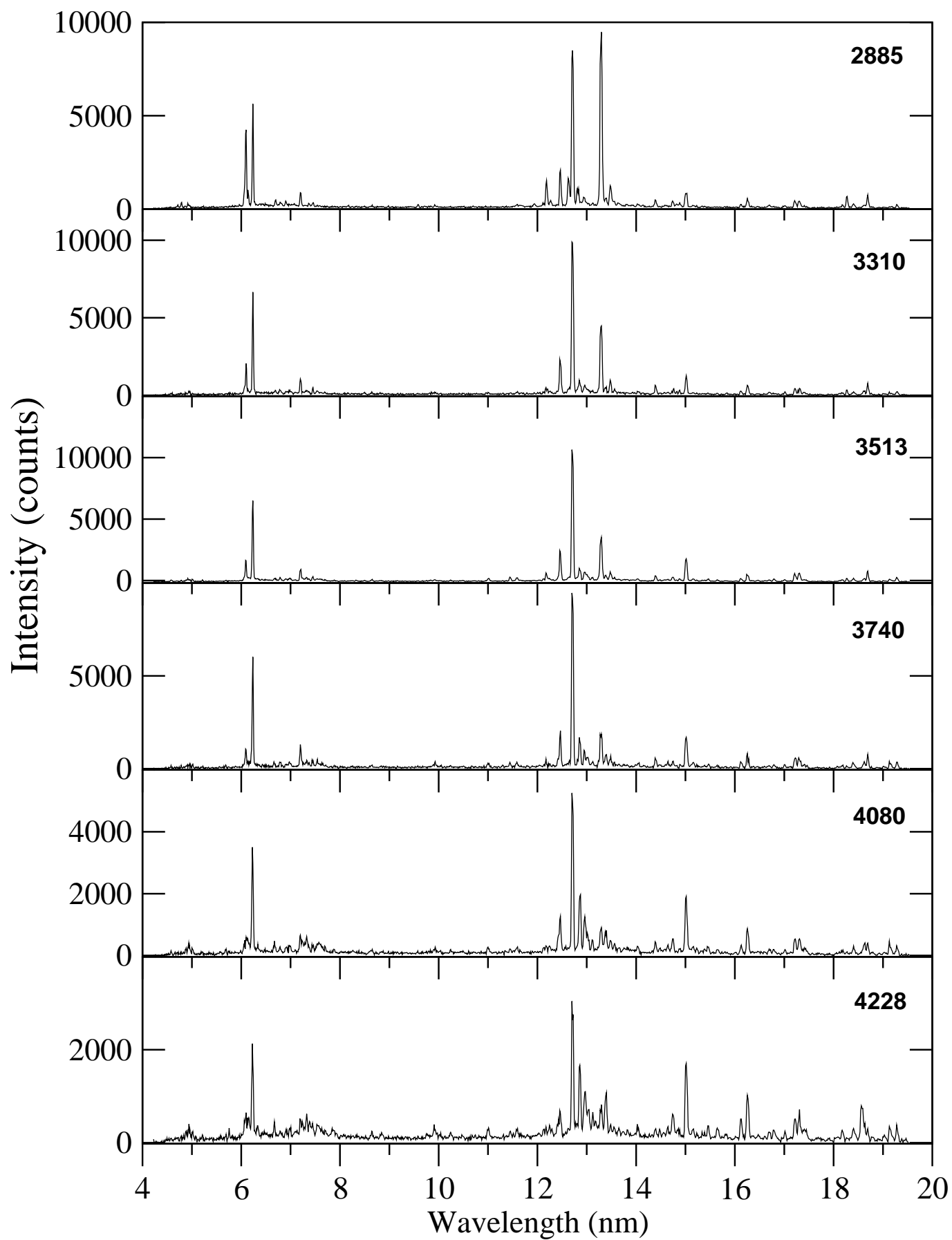


Figure 3. Experimental spectra for run B.

for the present work. Although the calculations are carried out in a relativistic jj-coupling scheme, we will also be using LS-coupling notation if this is more appropriate. As the CR modeling of non-Maxwellian plasmas, such as that of EBIT, is based on collisional cross sections rather than thermally-averaged rate coefficients, we created a database of cross sections for electron impact excitation, ionization, and radiative recombination. The cross sections of inverse processes were determined from the principle of detailed balance. Dielectronic recombination was not important in this experiment because the narrow electron-energy distribution function (EEDF) of the beam does not overlap with the resonant energies that are of importance for dielectronic capture. Also, three-body recombination can be completely neglected under the present low-density conditions.

A total of about 5000 atomic levels for ionization stages from Br-like  $W^{39+}$  to Mn-like  $W^{49+}$  were included in our simulations. The EEDF of the electron beam was modeled by a Gaussian function with a full width at half-maximum of 60 eV. The results of the calculations were not sensitive to the beam energy width in the range of 30 eV to 60 eV, a range that covers that typical of an EBIT.

### 3.1. Atomic data accuracy

The assessment of the accuracy of the atomic data for highly-ionized tungsten is impeded by the lack of reliable experimental information, especially for collisional cross sections. Nonetheless, good agreement between the experimental and simulated x-ray spectra [3] provides a strong indication that the data generated by FAC are sufficiently accurate for our present purpose. One may generally expect higher precision for x-ray spectra simulations compared to the EUV case due to higher importance of correlation effects for EUV transitions between excited states. Nevertheless, as will be shown below, the simulated EUV spectra are also in good agreement with the measurements, both for line positions and for intensities. Another test of the FAC data is provided by the calculated ionization potentials (last column in Table 1), which are seen to differ from the recommended values of Ref. [13] by less than 0.2 %.

Although several papers calculating energy levels and radiative transition probabilities for [Ga] and [Ni] isoelectronic sequences were published recently (e.g., [16, 17, 18]), the most comprehensive large-scale calculation of atomic data and spectral line intensities for highly-ionized tungsten remains that by Fournier [19]. He used the fully relativistic parametric potential code RELAC [20, 21, 22] to produce spectroscopic data for ions of tungsten from Rb-like  $W^{37+}$  to Co-like  $W^{47+}$ .

### 3.2. Collisional-radiative modeling

The modeling was performed in the steady-state equilibrium approximation. In order to test the applicability of this approximation, we used NOMAD's ability to solve time-dependent rate equations. It was found that at an electron density of  $N_e = 10^{11} \text{ cm}^{-3}$ , a steady state for a W plasma is reached within few tenths of a second. As the trap is



reloaded typically every 4 s and observed continuously over the course of this time, our use of the steady-state approach is fully justified.

The calculated line intensities were convolved with a Gaussian function representing instrumental resolution and then multiplied by the transmission function. Figure 1 shows that below 7 nm the calculated transmission function drops rapidly, and in this region it is known less accurately than for longer wavelengths. We believe this uncertainty explains the somewhat larger discrepancies between intensities of the experimental and simulated spectra for shorter wavelengths.

The theoretical beam energy, used as a free parameter, was varied until a good fit of calculated and measured spectra was obtained. In all simulations the fitted theoretical energy was found to be smaller than the nominal beam energy. For instance, the energy difference for run A increases from several tens of eV at the lowest beam energies to about 500 eV at  $E = 3113$  eV. Such a difference is likely due to (i) space charge effects and (ii) charge exchange (CX) with neutrals or low-charged ions that are present in the EBIT. The space charge effect is estimated to reduce the energy of the beam electrons by not more than about 150 eV. While CX does not modify the beam energy, it effectively enhances recombination and thus shifts ionization balance toward lower charge states. To test the importance of CX, we performed a series of NOMAD runs using a simple approximation for the CX cross sections [23] and varying both the relative velocity of neutrals and W ions,  $v_{rel}$ , and the density of neutrals  $N_n$ . Although this modification significantly improved the agreement between experimental and fitted beam energies, the uncertainties in  $v_{rel}$  and  $N_n$  leave too many free parameters to unambiguously account for the effect of charge exchange. Improved models of EBIT trap dynamics are needed to determine these parameters. Hence, we excluded the CX contribution in our simulations.

Although CX affects the ionization balance, it is not likely to modify the relative line intensities within individual ion stages. The CX of neutrals with highly-charged ions results in preferential population of the shell with the principal quantum number  $n \approx Z_c^{3/4}$  [24] ( $Z_c$  is the ion charge), which gives  $n \approx 16-18$  for  $Z_c = 40-47$ . The ensuing radiative cascades are likely to smear out the population flux such that the *relative* populations of the low-excited states, which are responsible for the EUV emission, would not be modified. An indirect confirmation of this conclusion follows from our previous work on x-ray spectra [3] where the relative intensities of the  $W^{46+}$  lines originating from the  $n = 4-6$  shells were accurately calculated without involving charge exchange effects.

Finally, note that the variation of the electron beam energy by a few hundred eV does not noticeably affect the relative distribution of line intensities within a specific ion. Therefore, one could separately calculate spectral emission patterns for each ion and then derive the experimental ionization distribution using ratios of line intensities originating from different ionization stages.

#### 4. Experimental results and interpretation

All identified lines in the measured spectra of W (Figs. 1-3) represent  $\Delta n = 0$  transitions with principal quantum number  $n = 4$ . The low electron density of the EBIT plasma permits measurement of both allowed and forbidden lines. Strong impurity lines from the highly-ionized ions of oxygen and nitrogen are easily recognized by their almost constant intensity as the beam energy is changed. For instance, the lines at 15.01 nm, 17.21 nm, and 17.30 nm noted in the 2600A spectrum in Fig. 2, are the well known lines of O V and O VI [12]. The nitrogen was deliberately introduced as an ion-cooling agent. Also, the strong lines near 6 nm can be seen in the second and third grating orders. The high-order lines are indicated by dashed (second order) and dotted (third order) lines in Fig. 2.

The list of identified lines with measured wavelengths is given in Table 3. This table also includes other experimental [1] and calculated [19] wavelengths as well as the weighted oscillator strengths  $gf$ . The agreement between  $gf$  values calculated by RELAC [19] and FAC is excellent for almost all reported lines. The only exception is the magnetic-dipole (M1) line  $3d^9 \ ^2D_{3/2} - ^2D_{1/2}$  in the Co-like ion, where the discrepancy is about 20 %.

##### 4.1. Low-energy spectra: 2000 eV to 2600 eV

As seen from Table 1, the lowest beam energies of 2001 eV and 2083 eV are sufficient to produce ions up to Ge-like  $W^{42+}$ , with ground state configurations  $4s^2 4p^k$ ,  $k \geq 2$ . These ions have a relatively large number of  $n = 4$  excited states, which results in appearance of wide transition arrays near 6 nm and 13 nm, rather than well separated spectral lines. From comparison with the calculated spectra it was, nonetheless, possible to identify a new magnetic-dipole line  $4p^5 \ ^2P_{3/2} - 4p^5 \ ^2P_{1/2}$  in Br-like  $W^{39}$ .

A dramatic change in the appearance of the spectrum is seen in Fig. 1 when the beam energy is changed from 2083 eV to 2255 eV. At the higher energy, which is sufficient to reach all ionization stages up to Zn-like  $W^{44+}$  (yet not to produce a significant amount of this ion), individual spectral lines become more visible in the spectrum. The agreement between experimental and simulated spectra patterns is exemplified in Fig. 4. While the nominal beam energy was 2169 eV, the best theoretical fit, based on the relative intensities of lines from different W ions in the 12 nm to 14 nm region, was obtained for an energy of 2120 eV. Aside from impurity and second-order lines that are marked in Fig. 4 by crosses and stars, respectively, almost all measured lines can be matched to calculated ones from a visual comparison of line positions and their relative intensities. Moreover, the derived line identifications are well confirmed by the dependence of line intensities upon the beam energy.

As an example, consider in more detail the identification procedure for the strong lines between 12 nm and 14 nm shown in Fig. 4 (see also Table 3). Our collisional-radiative modeling shows that at the fitted energy of 2120 eV the most populated ions of tungsten have the following distribution: [Br] : [Se] : [As] : [Ge] = 0.01 : 0.10 : 0.42

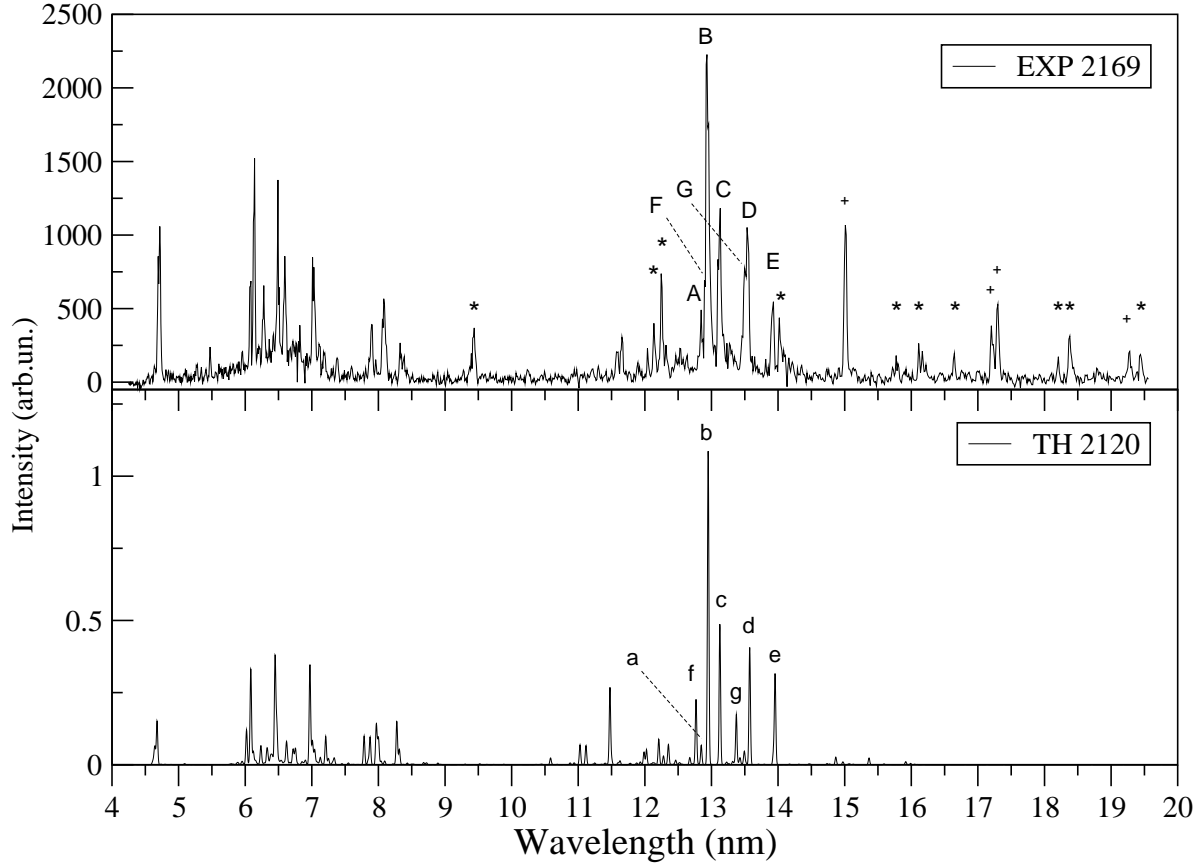


**Figure 4.** Comparison of the experimental (top) and calculated (bottom) spectra at the nominal beam energy of 2169 eV. The high-order lines are marked by stars, and the impurity lines are marked by crosses.

: 0.46, and thus one may expect to observe strong emission in  $W^{41+}$  and  $W^{42+}$ . The strongest lines are marked by letters A through E in Fig. 4. Both the positions and relative intensities of the lines B, C, D, and E very well agree with the calculated ones ( $b$ ,  $c$ ,  $d$ ,  $e$ ), and therefore these four lines can be identified as follows: B - electric-quadrupole (E2)  $4p^2\ ^3P_0 - 4p^2\ ^1D_2$  transition in Ge-like  $W^{42+}$ , C - M1  $4p^3\ ^2D_{3/2} - 4p^3\ ^2D_{5/2}$  transition in As-like  $W^{41+}$ , D - M1  $4p^2\ ^3P_0 - 4p^2\ ^3P_1$  transition in  $W^{42+}$ , E - M1  $4p^3\ ^2D_{3/2} - 4p^3\ ^4S_{3/2}$  transition in  $W^{41+}$ . This identification is strengthened by the fact that, as seen from Fig. 1, lines C and E become relatively weaker than lines B and D as the beam energy increases. In Ref. [1] line D was associated with the Ga-like ion.

The assignment of quantum numbers for the  $W^{41+}$  levels is highly problematic due to very strong mixing of the basis states in the ground configuration. For instance, although the ground level is designated  $4s^2 4p^3\ ^2D_{3/2}$ , it actually has only 26 %  $^2D$  character [6].

The theoretical spectrum in Fig. 4 shows the presence of two other lines,  $f$  and  $g$ , which correspond to transitions  $4p^2\ ^3P_1 - 4s 4p^3\ ^3P_2$  and  $4p^2\ ^1D_2 - 4s 4p^3\ ^3P_2$ , in the Ge-like ion $\ddagger$ . Although it may appear that the experimental line A should be associated with

$\ddagger$  The upper level, which in fact is the lowest odd level with  $J = 2$ , is identified as

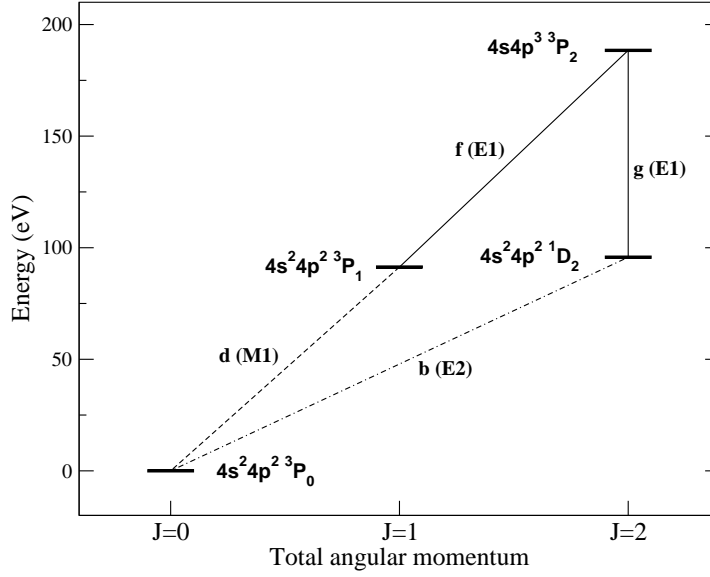


**Figure 5.** Four lowest energy levels in Ge-like  $W^{42+}$ . The line labels (see Fig. 4) and transition multipoles are indicated next to the lines.

$f$ , this line can also be seen at lower energy and therefore is assigned to the transition  $4p^4 \ ^3P_2 - 4p^4 \ ^1D_2$  in Se-like  $W^{40+}$ . In order to find the experimental lines corresponding to  $f$  and  $g$ , one can make use of the following observation. The *four* strongest lines from  $W^{42+}$  near 13 nm, which are listed in Table 3, connect *four* levels (Fig. 5). Therefore, if one denotes the transition energy corresponding to line  $a$  as  $E(a)$ , then  $E(f) + E(d) = E(b) + E(g)$ , or  $E(b) - E(d) = E(f) - E(g)$ . Hence, as  $E(b) - E(d)$  can be easily determined from the experimental spectra, the other pair of lines can be found using the derived difference of wavelengths. While no isolated spectral lines near 13 nm seem to satisfy this condition, two blended structures on the short-wavelength shoulders of lines B and E indeed correspond to the derived separation. Therefore we tentatively identify this pair of lines, which are shown by the upper-case letters F and G in Fig. 4, with the transitions  $f$  and  $g$ .

As the beam energy varies between 2000 eV and 2600 eV, new ionization stages of W appear in the spectrum and the spectral patterns change markedly. Figure 6 (top) shows the measured spectrum at 2429 eV from 12 nm to 14 nm. The best fit was obtained for a fitted beam energy of 2270 eV (bottom of Fig. 6), and one can see a good correspondence between the simulations and the measured spectrum. At this energy, the lines from the Ge- and Ga-like ions are the strongest, and their identification poses no difficulty (see Table 3). Since the beam energy exceeds the ionization potential of the Ga-like ion, the intercombination  $4s^2 \ ^1S_0 - 4s 4p \ ^3P_1$  line in Zn-like  $W^{44+}$  is also visible at 13.288 nm. One can see from this figure that the relative line intensities are calculated accurately for almost all lines. The only exception is the  $4s^2 4p \ ^2P_{1/2} - 4s 4p^2 \ ^4P_{1/2}$  transition in the Ga-like ion at 12.817 nm, for which the calculated intensity is too high  $4s(^2S_{1/2})4p^3(^2P_{3/2}^\circ) (1/2, 3/2)_2^\circ$  in Ref. [6].

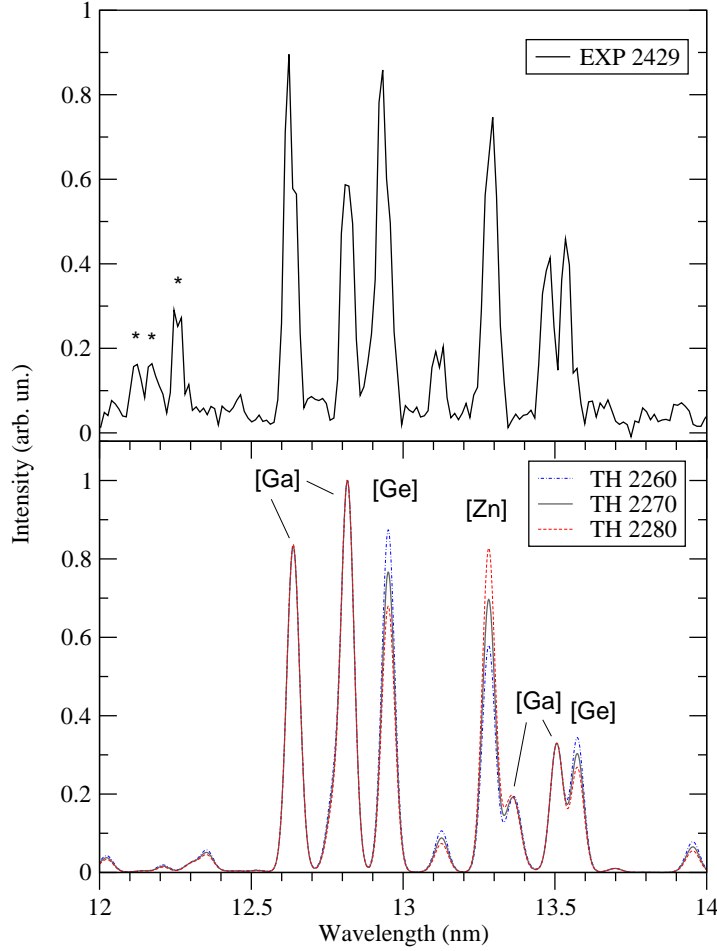


**Figure 6.** Comparison of the experimental (top) and calculated (bottom) spectra at the nominal beam energy of 2429 eV. The second-order lines are marked by stars.

by about a factor of two. Such a discrepancy was found for all other beam energies where this line is visible.

To illustrate the sensitivity of the simulated spectra to the beam energy, in Fig. 6 we also give results of the simulations at 2260 eV, 2270 eV, and 2280 eV, normalized to the peak of the 12.817 nm line in the Ga-like ion. A change of only 10 eV in the theoretical beam energy does not affect the intensities of the spectral lines within the same ion (cf. Ga-like lines at 12.629 nm, 12.817 nm, and 13.481 nm), but does drastically modify the relative intensities for different ions. This is most clearly seen when comparing the [Ge] 12.936 nm and the [Zn] 13.288 nm lines: the intensity ratio changes from 1.50 to 0.82 when the theoretical beam energy increases from 2260 eV to 2280 eV.

Although the line at 13.481 nm was identified as the [Ge]  $4p^2\ ^3P_0 - 4p^2\ ^3P_1$  transition in Ref. [1], it is evident both from this plot and from the variation of line intensity with the beam energy (Fig. 1) that it originates from the Ga-like ion. Accordingly, we identify it with the  $4s^24p\ ^2P_{3/2} - 4s4p^2\ ^4P_{5/2}$  transition.

#### 4.2. Medium-energy spectra: 2600 eV to 3500 eV

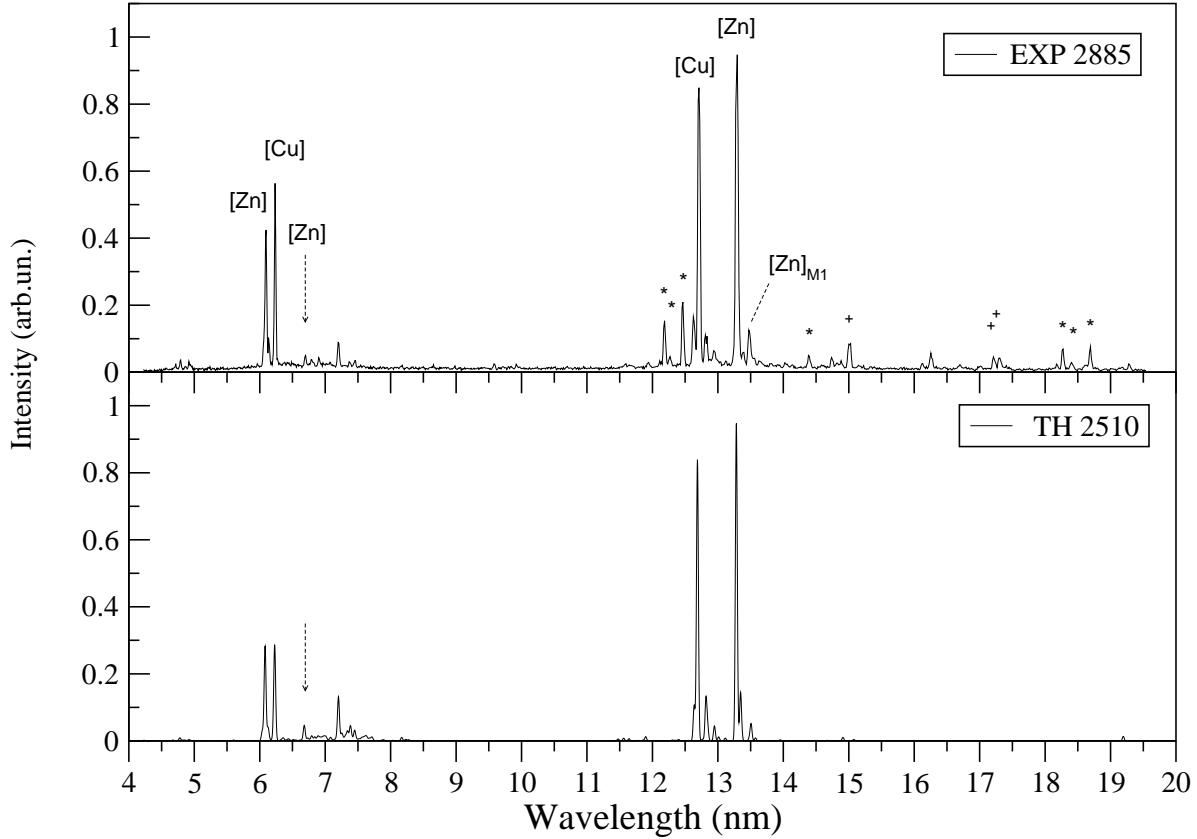
The spectra for the beam energies between 2600 eV and 3500 eV are dominated by a strong emission in the  $4s^2-4s4p$  and  $4s-4p$  lines from Zn- and Cu-like ions, respectively. The large difference between the ionization potentials of the Cu- and Ni-like ions is responsible for small modifications in ionization balance, and thus small variations in the spectral pattern. Although the energy of the beam is sufficient to produce Ni-like  $W^{46+}$ , the corresponding  $n = 4 - 4$  transitions are very weak as the total population of  $W^{46+}$  is still relatively small.

Figure 7 compares the experimental spectrum at 2885 eV with the simulated spectrum at 2510 eV. As already mentioned, we believe that this difference of 375 eV is due to CX and space-charge effects that are difficult to accurately account for. Other than that, the agreement in line positions and intensities is very good over the whole range. The well known intercombination  $4s^2\ ^1S_0 - 4s4p\ ^3P_1$  line (or  $4s^2\ (1/2, 1/2)_0 - 4s4p\ (1/2, 1/2)_1$  in jj-coupling) from the Zn-like ion and resonance  $4s_{1/2} - 4p_{1/2}$  line from the Cu-like ion are the most prominent. The other measured lines between 12.5 nm and 13.5 nm can also be unambiguously identified, including the magnetic-dipole  $4s4p\ ^3P_1 - 4s4p\ ^3P_2$  (or  $4s4p\ (1/2, 1/2)_1 - 4s4p\ (1/2, 3/2)_2$ ) line in [Zn]  $W^{44+}$  at 13.480 nm. The relative intensity of this line, which hereafter will be referred to as  $[Zn]_{M1}$ , remains approximately constant with respect to the intercombination line at 13.288 nm over a large range of energies indicating that it indeed originates from the Zn-like ion. This line was not observed in the tokamak spectrum [1].

Our identification of the  $[Zn]_{M1}$  line presents a problem with regard to some of the identifications of Zn-like lines identified in the LLNL EBIT measurements [5]. In Ref. [5], two Zn-like lines were identified as  $4s4p\ (1/2, 3/2)_2 - 4s4d\ (1/2, 5/2)_2$  at 4.45299(62) nm and  $4s4p\ (1/2, 1/2)_2 - 4s4d\ (1/2, 5/2)_2$  at 6.69301(40) nm. This implies a wavelength for  $[Zn]_{M1}$  of 13.305(6) nm, compared to our observed wavelength of 13.480(3) nm, a clear inconsistency. In Ref. [5] the 4.45299 nm line was observed with a relative intensity of 0.04, the same as that of the 6.69301 nm line. However, both our present calculations and those of Ref. [19] indicate that the 6.69301 nm line should be stronger by a factor of nearly 4. Since the upper level is the same for both lines, the calculated ratio is not sensitive to beam energy or other collisional effects. Since we observe the 6.69301 nm line (indicated by arrows in Fig. 7) as was observed in [5], we suspect that the problem rests with the 4.45299 nm line. (We are not able to observe this line due to the low transmission of our filter at this wavelength.) If we accept the identification of the 6.69301 nm line, our wavelength for  $[Zn]_{M1}$  implies a wavelength for  $4s4p\ (1/2, 3/2)_2 - 4s4d\ (1/2, 5/2)_2$  of 4.4724(4) nm, and it is likely that the identification in Ref. [5] will have to be revised.

#### 4.3. High-energy spectra: 3500 eV to 4228 eV

For beam energies greater than 3500 eV (Fig. 3), lines from Ni-like  $W^{46+}$  become more intense due to a larger relative population of this ion and also cascades from highly-



**Figure 7.** Comparison of the experimental (top) and calculated (bottom) spectra at nominal beam energy of 2885 eV. High-order lines are marked by stars, and impurity lines are marked by crosses. Arrows indicate the  $4s4p (1/2, 1/2)_2 - 4s4d (1/2, 5/2)_2$  line in the Zn-like ion at 6.69301 nm (see text).

excited levels that are populated by electron excitation. The lines from the lower ( $Z_c < 44$ ) charge states are barely visible, while the resonance  $4s - 4p$  line in the Cu-like ion is still the strongest.

The best fit for the measured spectrum at 4228 eV was obtained at a theoretical beam energy of 4100 eV (see Fig. 8). This energy is above the ionization threshold of the Ni-like  $W^{46+}$  and thus one may expect to find some lines from the Co-like ion  $W^{47+}$ . The strongest calculated line in  $W^{47+}$  corresponds to the M1 transition  $3d^9 \ ^2D_{5/2} - 3d^9 \ ^2D_{3/2}$  with theoretical wavelength of 18.640 nm. Indeed, the measured spectrum contains a strong line at  $18.578 \pm 0.002$  nm, which is absent at lower energies. We therefore identify this as the [Co] M1 transition. Twenty years ago Ekberg et al. [25], using observed wavelengths for the  $3p^6 3d^9 \ ^2D_{5/2} - 3p^5 3d^{10} \ ^2P_{3/2}$  and  $3p^6 3d^9 \ ^2D_{3/2} - 3p^5 3d^{10} \ ^2P_{3/2}$  transitions in lower-charged ions of the isoelectronic sequence, predicted a wavelength for the  $\ ^2D_{5/2} - \ ^2D_{3/2}$  transition in  $W^{47+}$  to be  $18.541 \pm 0.032$  nm. The weaker structure at the red wing of this line is the [Cu] 6.234 nm line [5] in the third order.

The  $n = 4 - 4$  lines of the Ni-like ion are the most prominent in the 4228 eV spectrum. The wide transition array between 6.5 nm and 8 nm is mainly due to the

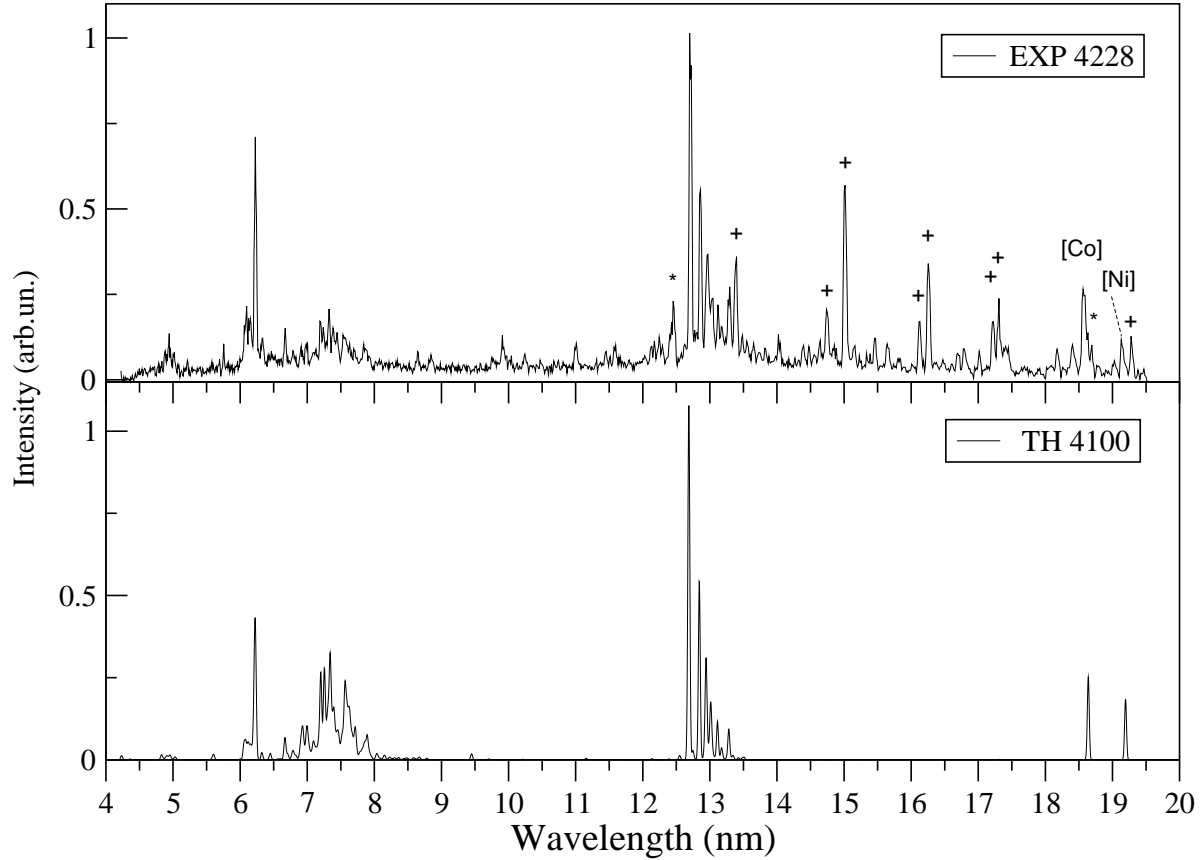


**Figure 8.** Comparison of the experimental (top) and calculated (bottom) spectra at the nominal beam energy of 4228 eV. The high-order lines are marked by stars, and the impurity lines are marked by crosses.

$3d^9 4p - 3d^9 4d$  and  $3d^9 4d - 3d^9 4f$  transitions in this ion, although it also includes tens of overlapping lines from the Cu-like ( $4p - 4d$ ) and Co-like ( $3d^8 4p - 3d^8 4d$  and  $3d^8 4d - 3d^8 4f$ ) ions. Although a good correspondence between the experimental and calculated spectral features can be seen, identification of individual lines is not possible with our spectral resolution.

The well-resolved lines near the [Cu]  $4s_{1/2} - 4p_{1/2}$  line at 12.7118 nm, listed in Table 3, are mainly due to the  $3d^9 4s - 3d^9 4p$  transitions in  $W^{46+}$ . According to our calculations, there are only six strong  $3d^9 4s - 3d^9 4p$  lines between 12.5 nm and 13.5 nm. The  $(5/2, 1/2)_3 - (5/2, 1/2)_3$  transition is completely blended with the [Cu] 12.7118-nm line, while the  $(3/2, 1/2)_1 - (3/2, 1/2)_2$  and  $(5/2, 1/2)_3 - (5/2, 1/2)_2$  lines differ by only 0.003 nm and thus cannot be resolved. The former of these two lines has a factor of three higher intensity than the latter, and therefore it is for this transition that the experimental wavelength is listed in Table 3. The remaining three lines in the Table are reliably resolved in the measured spectrum. The [Zn] intercombination  $4s^2 - 4s4p$  line at 13.2878 nm is still seen in the spectrum, although this ion is present at only about 0.3 % of the total population.

At longer wavelengths, a line at 19.1488 nm was identified as the M1 transition



$3d^9 4s (3/2, 1/2)_1 - 3d^9 4s (5/2, 1/2)_2$  in  $W^{46+}$ . In Ref. [3] we found that the decay of the upper level  $3d^9 4s (5/2, 1/2)_2$  through this process is crucially important for the accurate modeling of intensities of the  $3d^{10} - 3d^9 4s$  forbidden lines at 0.8 nm (see also [26]). Of course, this transition also substantially affects the population of the lower level  $3d^9 4s (3/2, 1/2)_1$ .

## 5. Conclusions

We presented the measurements of the EUV spectra of highly-charged ions of tungsten in the spectral range from 4 nm to 20 nm, emphasizing the study of spectral features above 12 nm. Implementing advanced collisional-radiative modeling based on extensive accurate sets of atomic data, we were able to identify almost all observed spectral lines. Some of those are newly reported here. Additional independent studies would be valuable in the case of the anomalous intensity observed for the Ga-like line at 12.817 nm, the wavelengths of the poorly resolved Ge-like E1 lines near 13 nm, and the likely previous misidentification of a Zn-like line at 4.45299 nm [5].

## Acknowledgments

This work was supported in part by the Office of Fusion Energy Sciences of the U. S. Department of Energy. We are grateful to A.E. Kramida for valuable discussions.

## References

- [1] Pütterich T, Neu R, Biedermann C, Radtke R and ASDEX Upgrade Team 2005 *J. Phys. B: At. Mol. Phys.* **38** 3071.
- [2] Assmussen K, Fournier KB, Laming JM, Neu R, Seely JF, Dux R, Englehardt W, Fuchs JC and ASDEX Upgrade Team 1998 *Nuclear Fusion* **38** 967.
- [3] Ralchenko Yu, Tan JN, Gillaspay JD, Pomeroy JM and Silver E 2006 *Phys. Rev. A* **74** 042514.
- [4] Blagojević B, Le Bigot E-O, Fahy K, Aguilar A, Makonyi K, Takács E, Tan JN, Pomeroy JM, Burnett JH, Gillaspay JD and Roberts JR 2005 *Rev. Sci. Instrum.* **76** 083102.
- [5] Utter SB, Beiersdorfer P and Träbert E 2002 *Can. J. Phys.* **80** 1503.
- [6] Kramida AE 2007 *At. Data and Nucl. Data Tables*, to be published; Kramida AE and Shirai T 2006 *J. Plasma and Fusion Res.* **7** 334.
- [7] Takács E, Meyer ES, Gillaspay JD, Roberts JR, Chantler CT, Hudson LT, Deslattes RD, Brown CM, Laming JM, Dubau J and Inal MK 1996 *Phys. Rev. A* **54** 1342.
- [8] Fahy K, Sokell E, O'Sullivan G, Aguilar A, Pomeroy JM, Tan JN, and Gillaspay JD 2007 *Phys. Rev. A* **75** 032520.
- [9] Gillaspay JD 1997 *Phys. Scr.* **T71** 99.
- [10] Brown IG, Galvin JE, Galvin BF and MacGill RA 1986 *Rev. Sci. Instrum.* **57** 1069.
- [11] Harada T and Kita T 1980 *Appl. Opt.* **19** 3987.
- [12] Ralchenko Yu, Jou F-C, Kelleher DE, Kramida AE, Musgrove A, Reader J, Wiese WL and Olsen K 2006 *NIST Atomic Spectra Database (version 3.1.0)*, [Online]. Available: <http://physics.nist.gov/asd3> [2007, January 15]. National Institute of Standards and Technology, Gaithersburg, MD.
- [13] Kramida AE and Reader J 2006 *At. Data and Nucl. Data Tables*, **92** 457.
- [14] Ralchenko YuV and Maron Y 2001 *J. Quant. Spectrosc. Radiat. Transfer* **71** 609.

- [15] Gu MF 2004 *14th APS Topical Conference on Atomic Processes in Plasmas, AIP Proceedings vol 730* (Melville:AIP Press).
- [16] Quinet P, Biémont E, Palmeri P and Träbert E 2007 *At. Data and Nucl. Data Tables* **93** 167.
- [17] Safronova UI, Cowan TE and Safronova MS 2006 *Phys Lett A* **348** 293.
- [18] Dong CZ, Fritsche S and Xie LY 2003 *J. Quant. Spectrosc. Radiat. Transfer* **76** 447.
- [19] Fournier KB 1998 *At. Data and Nucl. Data Tables* **68** 1.
- [20] Klapisch M 1971 *Comp. Phys. Commun.* **2** 239.
- [21] Aymar M, Crance M and Klapisch M 1970 *J. Phys. (Paris)*, **31** C4.
- [22] Klapisch M, Schwob JL, Fraenkel B and Oreg J 1977 *J. Opt. Soc. Am.* **67** 148.
- [23] Elton RC 2004 *X-Ray Lasers* (Boston:Academic Press).
- [24] Janev RK, Presnyakov LP and Shevelko VP 1985 *Physics of Highly Charged Ions* (Berlin:Springer-Verlag).
- [25] Ekberg JO, Feldman U, Seely JF, Brown CM, Reader J and Aquista N 1977 *J. Opt. Soc. Am. B* **4** 1913.
- [26] Ralchenko Yu 2007 *J. Phys. B: At. Mol. Phys.* **40** F175.

**Table 3.** Measured spectral lines of highly-ionized tungsten (wavelengths are in nm). We use notation  $a[b]$  for  $a \cdot 10^b$ . The experimental uncertainties for wavelengths are given in parentheses.

Ion	Transition	Type	$gf$ (Theory)		$\lambda$ (Exper.)		$\lambda$ (Theory)		New line
			Ref. [19]	this work	this work	Ref. [1]	Ref. [19]	this work	
W <sup>39+</sup> [Br]	$4p^5 \ ^2P_{3/2} - 4p^5 \ ^2P_{1/2}$	M1	3.94[-5]	4.12[-5]	13.474(4)		13.35922	13.347	new line
W <sup>40+</sup> [Se]	$4p^4 \ ^3P_2 - 4p^4 \ ^1D_2$	M1	4.85[-5]	5.18[-5]	12.852(5)	12.864(5)	12.83020	12.847	new line
	$4p^4 \ ^3P_2 - 4p^4 \ ^3P_1$	M1	5.10[-5]	5.23[-5]	13.488(9)	13.487(5)	13.49228	13.493	
W <sup>41+</sup> [As]	$4p^3 \ ^2D_{3/2} - 4p^3 \ ^2D_{5/2}$	M1	1.90[-5]	2.28[-5]	13.124(4)	13.121(5)	13.23688	13.127	new line
	$4p^3 \ ^2D_{3/2} - 4p^3 \ ^4S_{3/2}$	M1	8.16[-5]	8.23[-5]	13.914(5)	13.896(5)	14.10290	13.956	
W <sup>42+</sup> [Ge]	$4s^2 4p^2 \ ^3P_1 - 4s 4p^3 \ ^3P_2$	E1	1.50[-1]	1.56[-1]	12.895(4)	12.912(5)	12.73583	12.768	tentative
	$4s^2 4p^2 \ ^3P_0 - 4s^2 4p^2 \ ^1D_2$	E2	1.78[-6]	1.87[-6]	12.941(4)	12.945(5)	13.05679	12.951	tentative
	$4s^2 4p^2 \ ^1D_2 - 4s 4p^3 \ ^3P_2$	E1	1.25[-1]	1.36[-1]	13.495(6)	13.475(5)	13.35610	13.373	
	$4s^2 4p^2 \ ^3P_0 - 4s^2 4p^2 \ ^3P_1$	M1	4.09[-5]	4.09[-5]	13.545(4)		13.70953	13.574	13.475 nm in [1]
W <sup>43+</sup> [Ga]	$4s^2 4p \ ^2P_{1/2} - 4s^2 4p \ ^2P_{3/2}$	M1	4.17[-5]	4.37[-5]	12.629(3)	12.639(5)	12.60060	12.638	new line
	$4s^2 4p \ ^2P_{1/2} - 4s 4p^2 \ ^4P_{1/2}$	E1	1.38[-1]	1.50[-1]	12.817(4)	12.824(5)	12.70610	12.817	
	$4s^2 4p \ ^2P_{3/2} - 4s 4p^2 \ ^4P_{5/2}$	E1	2.53[-1]	2.29[-1]	13.481(10)		13.45507	13.506	
W <sup>44+</sup> [Zn]	$4s^2 \ ^1S_0 - 4s 4p \ ^3P_1$	E1	1.38[-1]	1.39[-1]	13.288(3)	13.287(5)	13.20751	13.149	new line
	$4s 4p \ ^3P_1 - 4s 4p \ ^3P_2$	M1	5.64[-5]	5.57[-5]	13.480(3)		13.36069	13.345	
W <sup>45+</sup> [Cu]	$4s \ ^2S_{1/2} - 4p \ ^2P_{1/2}$	E1	2.35[-1]	2.29[-1]	12.712(3)	12.720(5)	12.62740	12.688	
W <sup>46+</sup> [Ni]	$3d^9 4s (3/2, 1/2)_1 - 3d^9 4p (3/2, 1/2)_2$	E1	2.98[-1]	2.96[-1]	12.860(3)		12.74701	12.841	new line
	$3d^9 4s (5/2, 1/2)_3 - 3d^9 4p (5/2, 1/2)_2$	E1	4.56[-1]	4.54[-1]			12.78189	12.844	blended
	$3d^9 4s (5/2, 1/2)_2 - 3d^9 4p (5/2, 1/2)_3$	E1	4.55[-1]	4.52[-1]	12.958(4)		12.84375	12.944	new line
	$3d^9 4s (3/2, 1/2)_2 - 3d^9 4p (3/2, 1/2)_2$	E1	2.73[-1]	2.71[-1]	13.019(6)		12.92460	13.012	new line
	$3d^9 4s (5/2, 1/2)_2 - 3d^9 4p (5/2, 1/2)_2$	E1	1.08[-1]	1.07[-1]	13.113(3)		13.03312	13.112	new line
	$3d^9 4s (5/2, 1/2)_2 - 3d^9 4s (3/2, 1/2)_1$	M1	3.98[-5]	3.98[-5]	19.149(2)		19.15539	19.195	new line
W <sup>47+</sup> [Co]	$3d^9 \ ^2D_{3/2} - 3d^9 \ ^2D_{1/2}$	M1	5.15[-5]	3.43[-5]	18.578(2)		18.62292	18.640	new line

Spectral lines of W<sup>39+</sup> to W<sup>47+</sup> in the 12 nm to 20 nm region